Strengthening mechanism of friction stir processed and post heat treated NiAl bronze alloy: Effect of rotation rates

Yuting Lv [a, b], Yang Ding [a], Yuanfei Han [a], Lai-Chang Zhang [c], Liqiang Wang [a, b] *, Weijie Lu [a, b] *

[a] State Key Laboratory of Metal Matrix Composites, Shanghai Jiao Tong University, Shanghai 200240, PR China

[b] Collaborative Innovation Center for Advanced Ship and Deep-Sea Exploration, Shanghai 200240, PR China

[c] School of Engineering, Edith Cowan University, 270 Joondalup Drive, Joondalup, Perth, WA 6027, Australia

Corresponding author. Tel.: +86 21 34202641; fax: +86 21 34202749.

E-mail address: luweijie@sjtu.edu.cn, wang_liqiang@sjtu.edu.cn

Abstract:

In this work, NiAl bronze (NAB) alloys were subjected to friction stir processing (FSP) at a constant traverse speed of 100 mm/min and rotation rates of 600 rpm, 800 rpm, 1000 rpm and 1200 rpm, respectively. Thereafter, heat treatment was performed at 675 °C for 2 hours. The effects of rotation rates on strengthening mechanisms of friction stir processed and post heat treated NAB alloy were studied. The results showed that friction stir processed NAB alloy microhardness was increased as the rotation rate increased. During friction stir processing, martensite nanotwins could be formed due to high strain rates and

peculiar martensitic structures of NAB alloys. A rotation rate increase, increased peak temperatures and strain rates in friction stir processed NAB alloys, leading to a significant amount of martensite nanotwins formation. As rotation rates increased from 600 rpm to 1200 rpm, in addition to grain refinement effects, the strengthening mechanism of friction stir processed NAB alloys gradually changed from secondary phase strengthening to solid solution, dislocations and nanotwin strengthening. During post heat treatment, discontinuous static recrystallization occurred and β' phase decomposed into α and κ phases. Highest microhardness values were obtained at the rotation rate of 800 rpm and the uniformly distributed second phases formed during friction stir processing contributed mainly to higher microhardness.

Keywords: NiAl bronze (NAB); Friction stir processing; Post heat treatment; Strengthening mechanism; Microstructure.

1. Introduction:

The Nickel-aluminum bronze (NAB) alloy is a binary copper-aluminum system microalloyed with nickel, iron and manganese elements. Due to the excellent combination of high strength and corrosion resistance, this alloy is widely used for ship propeller, pump and valves [1]. The cast NAB alloy presents complex microstructures mainly consisting of coarser Widmanstätten α phases, intermetallic phases (κ_i, κ_{ii}, κ_{iii} and κ_{iv}) and retained β phase (β' phase) [2]. These complex

microstructures are a disadvantage for both mechanical properties and corrosion resistance of as cast NAB alloys. Coarser Widmanstätten α grains in as cast NAB alloys significantly decrease the tensile strength [3] and the β' phase can accelerate fatigue crack growth [4]. Also, eutectoid $\alpha+\kappa_{iii}$ structure results in as cast NAB alloys being easily subjected to selective phase corrosion [5]. Maximum Volta potential differences between α and κ_i phases can reach 70mV, increasing the galvanic corrosion of as cast NAB alloys [6]. In addition, defects of shrinkage porosities are prone to appear due to poor casting performance [1], making fatigue cracks easy to initiate [7].

In order to eliminate shrinkage porosities and to improve mechanical properties of cast NAB alloy, several techniques have been adopted such as equal channel angular extrusion [8], laser surface melting [9, 10], and friction surfacing [11]. These methods can produce refined and uniformly distributed microstructures, significantly improving mechanical properties and corrosion resistance of as cast NAB alloys. Recently, a new surface treatment method called friction stir processing has been paid more and more attentions due to its energy efficiency, environment friendliness, and versatility [12]. During friction stir processing, alloys undergoes severe plastic deformation combined with elevated temperatures, resulting in fine and homogeneous microstructures, significantly enhancing mechanical properties of NAB alloys [12].

The applications of friction stir processing on NAB alloy have been reported in many studies [13-16]. Oh-ishi et al. reported that highly refined and recrystallized grains with grain size of 2 μm were formed in friction stir processed NAB alloys. It was considered that κ_{ii} and κ_{iv} particles acted as the nucleation sites for as cast NAB alloy grain recrystallization [17]. Menon et al. [16] reported that friction stir processed NAB alloy strengthening mechanisms involved grain refinement, solid solutions, precipitations and dislocation strengthening. Many martensite nanotwins were also formed in hot rolled and friction stir processed NAB alloys [18, 19]. These nanotwins acted as a grain boundary and increased the mechanical properties of NAB alloy [18]. Lu et al. reported that nanotwins were formed when Cu-Al alloys were deformed at higher strain rate and lower temperature [20]. They attributed the formation of the nanotwins to lower stacking fault energies of Cu-Al alloys [21]. However, nanotwins were also formed in friction stir processed NAB alloys, being deformed at higher strain rates and temperatures. The reason of formation of the nanotwins in friction stir processed NAB alloys has rarely been studied.

The martensite phases produced during friction stir processing have a detrimental effect on corrosion resistance of NAB alloys. Lenard et al. reported that pit corrosion occurred on β' phases following long time exposure to sea water [22]. Song et al considered that martensitic

structures and direct contact with cathodic second phases were responsible for the corresponding worse corrosion resistance [23]. In addition, rigid clamping was utilized during friction stir processing, which is a large restraint for the welded plates. Such restraint impeded the contraction of friction stir processed regions during cooling down, therefore leading to higher residual stresses in friction stir processed samples [12]. The existence of high residual stresses was undoubtedly detrimental to mechanical properties. During actual production, post heat treatment is an effective method for residual stress formation reduction during plastic deformation and β' phase contents in NAB alloy [24]. The fine κ phases formed during heat treatment can also improve erosion-corrosion resistance of NAB alloy [25]. However, to our knowledge, post heat treatment of friction stir processed NAB alloys was rarely studied.

Therefore, in this work, NAB alloys were subjected to friction stir processing and then post heat treatment was performed at 675°C for 2 hours. The reason of formation of martensite nanotwins in friction stir processed NAB alloys and its evolution during post heat treatment were studied. Furthermore, four rotation rates were chosen, such as 600 rpm, 800 rpm, 1000 rpm and 1200 rpm for a strengthening mechanisms variations study, such as increased rotation rates in friction stir processed and post heat treated NAB alloys.

2. Experimental Procedure

The material used in this work was a Cu-9.5Al-4.2Ni-4Fe-1.2Mn (wt %) NAB alloy. The preparation processes of cast, forged and friction stir processed NAB alloys have been reported in detail in our previous studies [19]. The forged NAB alloy samples were subjected to friction stir processing at the same traverse speed (υ) of 100mm/min and under various rotation rates (ω) of 600rpm, 800rpm, 1000rpm and 1200 rpm, respectively. The corresponding friction stir processed samples were indicated as the FSP600, FSP800, FSP1000 and FSP1200. The post heat treatments for friction stir processed samples were carried out at 675 °C for 2 hours, followed by cooling in air. Accordingly, the post heat treated samples for FSP600, FSP800, FSP1000 and FSP1200 were indicated as PHT600, PHT800, PHT1000 and PHT1200, respectively.

The phase constituents were identified by a D8 ADVANCE X-ray diffractometer (XRD) with Cu Kα radiation at room temperature. The XRD patterns were recorded at a step size of 0.01° and a scanning speed of 3°/min on polished top surface with a distance of 0.5mm from friction stir processed surfaces. Previous studies indicated that most β' phases transformed into α and/ or κ phases following heat treatment [19]. Therefore, in this study, the integrated areas for α and κ diffraction peaks in the XRD spectra were determined with a peak-fitting program utilizing the Pearson VII function [22]. Based on integrated areas, the relative

volume fraction (V_f) of κ phases was calculated with the following equation [26, 27]:

$$V_{f(\kappa)} = A_\kappa/(A_\kappa + A_\alpha)$$

Where $V_{f(\kappa)}$ is the relative volume fraction and A_κ and A_α are the total integrated areas, corresponding to the α and κ phases, respectively.

Microstructural characteristics of friction stir processed and post heat treated NAB samples were examined with a JEM-2100F scanning electron microscope (SEM) equipped with electron backscatter diffraction (EBSD) and a JEM-200 EX transmission electron microscope (TEM). The sample preparation methods for SEM, EBSD, TEM were described in detail in aforementioned studies [18, 19, 28]. It was noted that stir zones of friction stir processed NAB alloys present inhomogeneous microstructures due to different deformation degrees and peak temperatures in various subregions of friction stir processed samples [13]. In this study, all microstructures were acquired from the same subregion at a distance of 0.5mm from the top surfaces. Vickers micro-hardness values were measured on polished cross-sections at a distance of 0.5mm from the top surfaces with an automated tester with a 500 g load and a dwelling time of 15seconds. Each microhardness value was averaged from four tests.

3. Results

3.1 Structural characteristics

In Fig. 1(a), the XRD patterns of friction stir processed and post heat treated NAB alloys processed under various rotation rates are presented. Fig. 1(b) shows the magnified XRD pattern of a post heat treated NAB alloy between 42º-45º. Compared to post heat treated NAB alloys, all friction stir processed NAB samples displayed lower (Fe, Ni) Al peaks in the XRD profiles. This indicated that the κ phases had been dissolved into Cu matrix to form a solid solution during friction stir processing [29]. After post heat treatment, most β' phases transformed to α and/or κ phases, possibly missed in the XRD patterns. Therefore, the relative volume fractions (V_f) of α and κ phases in post heat treated NAB samples were estimated based on the XRD patterns, as shown in Table 1. The PHT800 sample has the lowest volume fraction of κ phases, implying that more κ phases are dissolved into the Cu matrix in the PHT800 sample, forming a solid solution. This result was consistent with SEM observation (Fig. 3(b)).

3.2 Microstructure

In Figs. 2 and 3, the SEM images of friction stir processed and post heat treated NAB alloys under various rotation rates are presented. As can been seen, the rotation rate had a significant influence on alloy microstructures. The microstructure of the FSP600 sample was composed of stream-like α, coarser κ and distorted retained β (β') phases. This indicated that severe plastic deformation occurred when the NAB alloy

were processed under 600 rpm rotation rate. As the rotation rate increased to 800 rpm (Fig. 2(b)), finer α and β' phases were observed and finer κ phases are uniformly distributed in the matrix and in β' phases. It is noted that the FSP800 processed on the forged NAB alloy displays different microstructures compared to that processed on as cast alloy [28]. However, finer κ phases are both observed on the matrix and β' phase. As the rotation rate further increased to 1000 rpm, microstructures were composed of Widmanstätten α and β' phases also. But fine κ phases were observed only in the β' phases (Fig. 2(c)). As the rotation rate increased to 1200 rpm, κ phases disappeared completely (Fig. 2(d)). This indicates that, the increase in the rotation rate results in the refinement of coarser α grains and solid solution of κ phases into NAB alloy matrix. Most κ phases were dissolved when NAB were processed under the rotation rate of 1200 rpm.

After post heat treatment, only a low amount of β' phase was observed in all post heat treated NAB samples, indicating that most β' phases had transformed into α and/ or κ phases during post heat treatment. More κ phases were observed in post heat treated alloys. Certain κ phases were located at grain boundaries and others were in matrix. In PHT600 samples, heterogeneity of coarse κ phases was observed (Fig. 3(a)), whereas κ phases in PHT800 samples were fine and uniformly distributed (Fig. 3(b)). As the rotation rate increased further, the grain size of κ

phases increased significantly. However, the relative volume fraction (V_f) of κ phases in PHT1200 samples was lower than the volume fraction in PHT1000 samples (Table 1), indicating that less and coarser κ phases were precipitated in PHT1200 sample during post heat treatment.

Fig. 4 shows the EBSD-IPF images of α grains in post heat treated NAB alloy. As can be seen, almost all zones in grain maps were identified as α phases, indicating that most of β' phases decomposed during post heat treatment. In Fig. 4(a), deformed α grains were observed in PHT600 samples. The grain size distribution map (not shown) reveals that most α grains in PHT600 sample had a grain size of 1-2.5 μm. As the rotation rate increased to 800 rpm, coarser α grains were formed (Fig. 4(b)). With further increasing the rotation rate, the grain size of α grains increased significantly (Fig. 4(c) and (d)). The fraction of coarser α grains with a grain size exceeding 5 μm was approximately 30% in PHT1200 sample. This occurred because a higher rotation rate could produce more dislocations and subboundaries, leading to higher energy storage in friction stir processed NAB alloys. The stored energy can accelerate nucleation and growth of recrystallization grains during post heat treatment [30].

3.2 Microhardness

Fig. 5 shows the microhardness distribution map of friction stir processed and post heat treated NAB alloy obtained at various rotation

rates. Here, we focus on the microhardness of stir zone in friction stir processed and post heat treated NAB alloy. As can be seen, the friction stir processed NAB alloys exhibited a significantly higher microhardness than post heat treated samples and microhardness increased with increasing rotation rate. The highest microhardness is discovered in the FSP1200 samples, which is 280Hv. After post heat treatment, highest microhardness is obtained in PHT800 sample, which is about 245Hv.

4. Discussion

4.1 Formation and transformation of martensite nanotwins during friction stir processing and post heat treatment

In Fig. 6(a), the TEM image of nanotwins in the FSP1000 sample is presented and the inset in Fig. 6(a) is the corresponding selected area electron diffraction pattern. As it can be observed, the average thickness of the nanotwins is approximately 15-30 nm and selected area electron diffraction displayed that the nanotwins is martensitic phase [31]. Sun et al. [31] reported that martensite phase exhibited disordered 3R structures. This structure was highly symmetrical [32] with long period stacking orders [33]. Fig. 6(b) shows the HRTEM image of a typical twinning morphology in Fig. 6(a). Domains “a” and “b” are two parts of the twins (indicated by a white line at the upper part of Fig. 6(b)). However, high densities of stacking faults in domain “a” were also observed. This indicated that these twins nucleated at the grain boundaries and grow into

the grain interiors via partial dislocation emission from grain boundaries [34]. It is also shown by molecular dynamic (MD) simulations that a twin can be nucleated following a stacking fault formation [29]. This occurred because a twin partial can be emitted on an adjacent plane to nucleate a twin when the partial dislocation has a same Burgers vector and operates as the initial leading partial dislocation. Martensite phases contain high densities of stacking faults because 3R martensite presents complex periodic stacking faults in its long period structure [33]. Moreover, NAB alloys had a lower stacking fault energy (SFE) because of the Al element addition [35]. It is well known that alloys with a low SFE present a higher propensity to deformation twins formation [29].

The TEM observation results on friction stir processed NAB alloys also displayed that the martensite nanotwins content was increased as rotation speeds increased. The combined effects of strain rate ($\dot{\varepsilon}$) and deformation temperature (T) can be expressed by the Zener-Holloman parameter [36, 37],

$$Z = (\dot{\varepsilon}) \exp(Q/RT) \text{ or } \ln Z = \ln \dot{\varepsilon} + \frac{Q}{RT}$$

Where R is the gas constant and Q is the related activation energy for deformation. Herein, the Q value for Cu alloys was 197kJ/mol [16, 18]. In this study, the material flow strain rate, $\dot{\varepsilon}$, during friction stir processing can be calculated by the following equation [38]

$$\dot{\varepsilon} = \frac{R_m \cdot 2\pi r_e}{L_e},$$

Where r_e and L_e are the effective (or average) radius and depth of the dynamically recrystallized zone. The effective radius was supposed to be equal to 0.78 of the friction stir processing tool boundary radius, r_o [36]. Similar assumption can also be applied to L_o. Regarding the friction stir processing tool used in this study, the effective boundary radius (r_o) and depth (L_o) were 2.25 and 2 mm, as shown in Fig. 7. It is noted that the average material flow rate of NAB alloys during friction stir processing was assumed being a simple linear flow. Therefore, R_m was calculated as the half rotational speed approximately of the pin, R_p, due to a certain extent of material rotation lagging effects during friction stir processing [38]. Therefore, for the FSP600, FSP800, FSP1000 and FSP1200 samples, $\dot{\varepsilon}$ was calculated as ~ 35.3s^{-1}, 47 s^{-1}, 59 s^{-1} and 70.7 s^{-1} respectively.

Since it was hard to directly measure the peak temperature during friction stir processing, a method was proposed by Oh-Ishi et al. [39] for local peak temperature estimation of friction stir processed NAB alloys with detailed microstructures. Based on detailed microstructural observation in the current work (Fig. 2), it can be inferred that the peak temperatures of FSP600, FSP800, FSP1000 and FSP1200 samples were ~800, 860, 930 and 1000°C, respectively [40]. Therefore, the ln Z for FSP600, FSP800, FSP1000 and FSP1200 samples could be calculated as ~25.6, 24.8, 23.8 and 22.9 respectively. It was found that all friction stir processed NAB alloys had similar ln Z values, indicating that ln Z values

had low influence on martensite nanotwins formation. That occurred because martensite nanotwins were formed due to combined effects of high strain rates and peculiar martensite structures of NAB alloys, the latter containing high densities of stacking faults. It was believed that high deformation temperatures accompanied by high strain rates would produce more martensite nanotwins. Therefore, the content of martensite nanotwins increased as rotation rates increased. Martensite nanotwins added the microhardness of friction stir processed NAB alloys by acting as a grain boundary and blocking lattice dislocation motion [37]. This phenomenon might have been one reason for microhardness of friction stir processed NAB alloys increase as rotation speeds increased.

After post heat treatment, as seen from Fig. 6(c), a large number of lamellar and rod-type precipitations were distributed in α matrix, implying that β' phases transformed into α and κ phases during post heat treatment. The κ phases were formed through discontinuous precipitation (DP) caused by grain boundary migration (indicated by red arrow in Fig. 6(c)) [41]. The precipitations might have increased in size during post heat treatment, leading to coarser κ phases formation (Fig. 6(d)).

4.2 The effect of rotation rate on the strengthening mechanism of friction stir processed and post heat treated NAB alloy

The microhardness of friction stir processed NAB alloy increases with increasing rotation rate (Fig. 5). After post heat treatment, the PHT800

sample exhibited higher microhardness compared to the PHT600 sample. With further increasing the rotation rate, the microhardness gradually decreased. In order to understand strengthening mechanisms of friction stir processed and post heat treated NAB alloys, we performed detailed TEM observations for friction stir processed and post heat treated samples, as shown in Fig. 8. Numerous fine κ phases with grain sizes of dozens of nanometers were observed in the FSP800 sample, whereas few fine κ phases were discovered in the FSP600 sample (Fig. 8(a), (c)). With further increasing the rotation rate to 1000 rpm, a significant amount of work hardening areas were formed and the fraction of fine κ phases reduced significantly (Fig. 8(b)). These results were consistent to SEM observations of friction stir processed NAB samples (Fig. 2). It can be inferred that κ phases fractured and dissolved as the rotation speed increased, due to significantly severe plastic deformation and gradual increase in local peak temperature. When the rotation rate exceeded 1000 rpm, most κ phases were dissolved (Fig. 2(d)). It is indicated that, as increasing the rotation rate from 600 rpm to 1200 rpm, accompanied by grain refinement, the strengthening mechanisms of friction stir processed NAB alloys gradually changed from secondary phases strengthening to solid solutions, dislocations and martensite nanotwins strengthening.

During post heat treatment, a discontinuous recovery and static recrystallization occurred, as shown in Fig. 6 and Fig. 8(d). The grain

sizes of α grains for post heat treated samples were estimated from the EBSD results. It was found that the average grain sizes of the α grains for PHT600, PHT800, PHT1000 and PHT1200 samples were approximately 1.9 μm, 2.3 μm, 2.6 μm and 3.1μm, respectively. It is indicated that the grain size increases with increasing rotation rate. This occurred because friction stir processed NAB alloys processed at higher rotation rates might produce more dislocations and subboundaries, increasing the nucleation driving force and growth of recrystallization grains [42]. Chang et al. reported that hardness and grain size had a Hall-Petch relation, presenting that the hardness of a polycrystalline material increases with decreasing grain size [43]. However, the PHT800 sample displayed a higher microhardness than the PHT600 sample. It is noted that the PHT800 sample had significantly more fine and uniformly distributed κ phases (Fig. 8(d)), being consistent with SEM observations of the PHT800 sample (Fig. 3(b)). Also, the PHT600 sample had non-uniform microstructures mainly composed of stream-like α, coarse κ_{ii} and fine κ_{iv} phases (Fig. 2(b)). This might explain the reason for the PHT800 sample exhibiting the highest microhardness among all post heat treated samples. The PHT600 sample had a higher volume fraction of κ phases (6.2%) than the PHT800 sample (5.1%), as seen from Table 1. In other words, more κ phases existed in the PHT600 sample. However,

finer and uniformly distributed κ phases in the PHT800 sample make a more contribution to its higher mechanical property.

5. Conclusion:

In this work, the effects of rotation rates on strengthening mechanisms of friction stir processing (FSP) and post heat treated NAB alloys were studied. The following conclusions can be drawn.

(1) The microhardness of friction stir processed NAB alloys increased as rotation rate increased. During friction stir processing, κ phases were gradually dissolved with increasing rotation rate. A significant amount of martensite nanotwins were formed due to high strain rates and peculiar martensite structures of NAB alloys. Increasing the rotation rate increased the peak temperatures and strain rates in friction stir processed NAB alloy, leading to form more martensite nanotwins.

(2) The strengthening mechanisms of friction stir processed NAB alloy involved grain refinement, secondary phases, solid solutions, dislocations and nanotwin strengthening. As the rotation rate increased from 600 rpm to 1200 rpm, accompanied with grain refinement effects, the strengthening mechanisms of friction stir processed NAB alloy change gradually from second phase strengthening to solid solution, dislocation and martensite nanotwin strengthening.

(3) After post heat treatment, most β' phases transformed into α and κ phases and discontinuous static recrystallization (DSRX) occurred.

The grain sizes of post heat treated NAB alloys gradually increased with increasing rotation rate. Highest microhardness value was obtained at the rotation rate of 800 rpm. Uniformly distributed secondary phases formed during friction stir processing make a main contribution to its higher microhardness.

Acknowledgements

Financial support of this research was jointly provided by 973 Program under Grant No: 2014CB046701. National Science Foundation under Grant No: 51302168 and 51674167, Shanghai Pujiang Program under Grant No: 15PJD017 and Science and Technology Planning Project of Jiujiang City.

Reference

[1] A. Jahanafrooz, F. Hasan, G.W. Lorrmer, N. Ridley, Microstructural development in complex nickel aluminum bronzes, Metall. Mater. Trans A. 14A (1982) 1951-1956.

[2] F. Hansan, A. Jahanafrooz, G.W. Lorimer and N. Ridley, The morphology, crystallography and chemistry of phases in as cast nickel aluminum bronze, Metall. Mater. Trans A. 13A (1982), 1337-1345.

[3] D.R. Ni, P. Xue, Z.Y. Ma, Effect of multiple-pass friction stir processing overlapping on microstructure and mechanical properties of as-cast NiAl bronze, Metall. Mater. Trans A. 42(8) (2011) 2125-2135.

[4] Y.T. Lv, M. Hu, L.Q. Wang, X.Y. Xu, Y.F. Han, W.J. Lu, Influences of heat treatment on fatigue crack growth behavior of NiAl bronze (NAB) alloy, J. Mater. Res. 30(20) (2015) 3041-3048.

[5] J.A. Wharton, K.R. Stokes, The influence of nickel–aluminium bronze microstructure and crevice solution on the initiation of crevice corrosion, Electrochim. Acta, 53(5) (2008) 2463-2473.

[6] D. Nakhaie, A. Davoodi, A. Imani, The role of constituent phases on corrosion initiation of NiAl bronze in acidic media studied by SEM–EDS, AFM and SKPFM, Corros. Sci. 80 (2014) 104-110.

[7] D. Taylor, J.F. Knott, Growth of fatigue cracks from casting defects in nickel–aluminium bronze, Metals Tech. 9 (1982) 221-228.

[8] L.L. Gao, X.H. Cheng, Microstructure and mechanical properties of Cu–10%Al–4%Fe alloy produced by equal channel angular extrusion, Mater. Des. 29 (2008) 904-908.

[9] C.H. Tang, F.T. Cheng, H.C. Man, Effect of laser surface melting on the corrosion and cavitation erosion behaviors of a manganese–nickel–aluminium bronze, Mater. Sci. Eng A. 373 (2004) 195-203.

[10] C.H. Tang, F.T. Cheng, H.C. Man, Improvement in cavitation erosion resistance of a copper-based propeller alloy by laser surface melting, Surf. Coat. Tech. 182 (2004) 300-307.

[11] S. Hanke, A. Fischer, M. Beyer, J. Santos, Cavitation erosion of

NiAl-bronze layers generated by friction surfacing, Wear, 273 (2011) 32-37.

[12] R.S. Mishra, Z.Y. Ma, Friction stir welding and processing, Mater. Sci. Eng. R: Reports, 50 (2005) 1-78.

[13] D.R. Ni, P. Xue, D. Wang, B.L. Xiao, Z. Y. Ma, Inhomogeneous microstructure and mechanical properties of friction stir processed NiAl bronze, Mater. Sci. Eng. A. 524 (2009) 119-128.

[14] K. Oh-Ishi, T.R. McNelley, The influence of friction stir processing parameters on microstructure of as cast nial bronze, Metall. Mater. Trans A. 36A (2005) 1575-1585.

[15] Q.N. Song, Y.G. Zheng, D.R. Ni, Z.Y. Ma, Corrosion and cavitation erosion behaviors of friction stir processed Ni-Al bronze: effect of processing parameters and position in the stirred zone, Corrosion, 70 (2014) 261-270.

[16] S.K. Menon, F.A. Pierce, B.P. Rosemark, K.Oh-Ishi, S. Swaminathan, T. R. McNelley, Strengthening mechanisms in NiAl bronze: hot deformation by rolling and friction stir processing, Metall. Mater. Trans. A. 43 (2012), 3687-3702.

[17] K. Oh-Ishi, T.R. McNelley, Microstructural modification of as-cast Ni Al bronze stir processing, Metall. Mater. Trans. A. 35A (2004) 2951-2961.

[18] Y.T. Lv, L.Q. Wang, Y.F. Han, X.Y. Xu, W.J. Lu, Investigation of

microstructure and mechanical properties of hot worked NiAl bronze alloy with different deformation degree, Mater. Sci. Eng A. 643 (2015) 17-24.

[19] Y.T. Lv, L.Q. Wang, X.Y. Xu, W.J. Lu, Effect of post heat treatment on the microstructure and microhardness of friction stir processed NiAl bronze (NAB) alloy, Metals. 5 (2015) 1695-1703

[20] L. Lu, X. Chen, X. Huang, K. Lu, Revealing the maximum strength in nanotwinned copper, Science 323(5914) (2009) 607-610.

[21] Y. Zhang, N.R. Tao, K. Lu, Effect of stacking-fault energy on deformation twin thickness in Cu–Al alloys, Scripta Mate. 60(4) (2009) 211-213.

[22] D.R. Lenard, C.J. Bayley, B.A. Noren, Electrochemical monitoring of selective phase corrosion of nickel aluminum bronze in seawater, Corro. Sci. Sect. 64(10) (2008) 764-772.

[23] Q.N. Song, Y.G. Zheng, D.R. Ni, Z.Y. Ma, Studies of the nobility of phases using scanning Kelvin probe microscopy and its relationship to corrosion behaviour of Ni–Al bronze in chloride media, Corro. Sci. 92 (2014) 95-103.

[24] R.P. Chen, Z.Q. Liang, W.W. Zhang, D.T. Zhang, Z.Q. Luo, Y.Y. Li, Effect of heat treatment on microstructure and properties of hot-extruded nickel-aluminum bronze, Metal. Soc. 17 (2007) 1254-1258.

[25] Z. Wu, Y.F. Cheng, L. Liu, W.J. Lv, W.B. Hu. Effect of heat

treatment on microstructure evolution and erosion–corrosion behavior of a nickel–aluminum bronze alloy in chloride solution, Corros. Sci. 98 (2015) 260-270.

[26] S.E. Haghighi, H.B. Lu, G.Y. Jian, G.H. Cao, D. Habibi, L.C. Zhang, Effect of α″ martensite on the microstructure and mechanical properties of beta-type Ti–Fe–Ta alloys, Mater. Des. 76 (2015), 47-54.

[27] S.E. Haghighi, Y.J. Liu, G.H. Cao, L.C. Zhang, Influence of Nb on the β→α" martensitic phase transformation and properties of the newly designed Ti-Fe-Nb alloys, Mater. Sci. Eng A. 60 (2016), 503-510.

[28] Y.T. Lv, L.Q. Wang, X.Y. Xu, Y.F. Han, W.J. Lu, Investigation of the microstructure and corrosion properties of friction stir processed cast NiAl bronze, Mater. Trans. 56 (2015) 1523-1529.

[29] K. Youssef, M. Sakaliyska, H. Bahmanpour, R. Scattergood, C. Koch, Effect of stacking fault energy on mechanical behavior of bulk nanocrystalline Cu and Cu alloys, Acta Mater. 59 (2011), 5758-5764.

[30] R. Nandan, T. DebRoy, H.K.D.H. Bhadeshia, Recent advances in friction-stir welding – process, weldment structure and properties, Prog. Mater. Sci. 53 (2008) 980-1023.

[31] Y.S. Sun. G.W. Lorimer and N. Ridley, Microstructure and its development in Cu-Al-Ni alloys, Mater. Trans. 21A (1988) 575-588.

[32] K. Otsuka, X.B. Ren, Mechanism of martensite aging effects and new aspects, Mater. Sci. Eng A. 312 (2001) 207-218.

[33] S. Kazanc, S. Ozgen, O. Adiguzel, Pressure effects on martensitic transformation under quenching process in a molecular dynamics model of NiAl alloy, Physica B: 334 (2003) 375-381.

[34] X.Z. Liao, Y.H. Zhao, S.G. Srinivasan, Y.T. Zhu, R.Z. Valiev, D.V. Gunderov, Deformation twinning in nanocrystalline copper at room temperature and low strain rate, Appl. Phys. Lett. 84 (2004), 592-594.

[35] X.X. Wu, X.Y. San, X.G. Liang, Y.L. Gong, X.K. Zhu, Effect of stacking fault energy on mechanical behavior of cold-forging Cu and Cu alloys, Mater. Des. 47 (2013), 372-376.

[36] Y.S. Li, Y. Zhang, N.R. Tao, K. Lu, Effect of the Zener–Hollomon parameter on the microstructures and mechanical properties of Cu subjected to plastic deformation, Acta Mater. 57 (2009), 761-772.

[37] N.R. Tao, K. Lu, Nanoscale structural refinement via deformation twinning in face-centered cubic metals,Scripta Mater. 60 (2009), 1039-1043.

[38] C.I. Chang, C. J. Lee, J.C. Huang, Relationship between grain size and Zener–Holloman parameter during friction stir processing in AZ31 Mg alloys, Scripta Mater. 51 (2004) 509-514.

[39] S. Swaminathan, K. Oh-Ishi, A.P. Zhilyaev, C.B. Fuller, B. London, M.W. Mahoney, T.R. McNelley, Peak stir zone temperatures during friction stir processing, Metall. Mater. Trans. A. 41A (2009) 631-640.

[40] J. Anantapong, V. Uthaisangsuk, S. Suranuntchai, A. Manonukul,

Effect of hot working on microstructure evolution of as-cast nickel aluminum bronze alloy, Mater. Des. 60 (2014) 233-243.

[41] I. Manna, S. K. Pabi, and W. Gust. Inter, Discontinuous reactions in solids, Mater. Rev, 46 (2001) 53-91.

[42] T. Sakai, A. Belyakov, R. Kaibyshev, H. Miura, J.J. Jonas, Dynamic and post-dynamic recrystallization under hot, cold and severe plastic deformation conditions, Prog. Mater. Sci. 60 (2014) 130-207.

[43] J. Yang, B.L. Xiao, D. Wang, Z.Y. Ma, Effects of heat input on tensile properties and fracture behavior of friction stir welded Mg–3Al–1Zn alloy, Mater. Sci. Eng A. 527(3) (2010) 708-714.

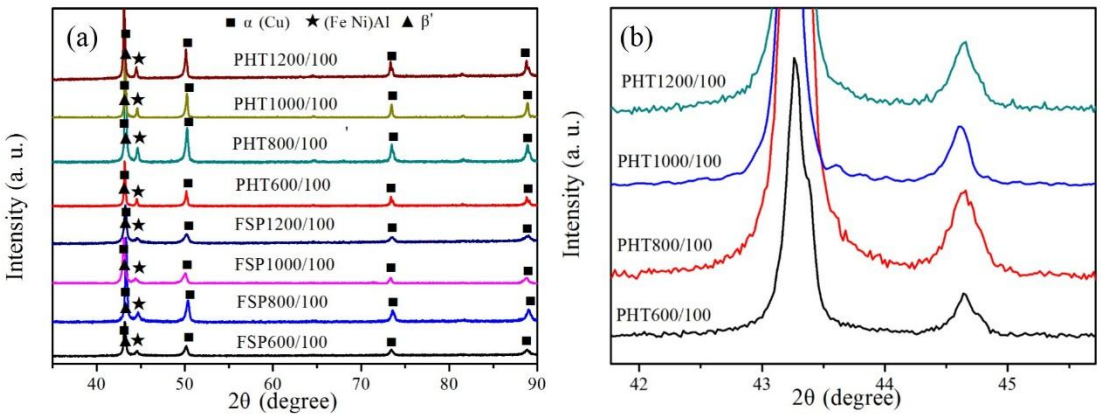

Fig. 1 (a) shows XRD patterns of the friction stir processed and post heat treated NAB alloy, (b) is magnified XRD pattern of post heat treated NAB alloy between 42º-45º.

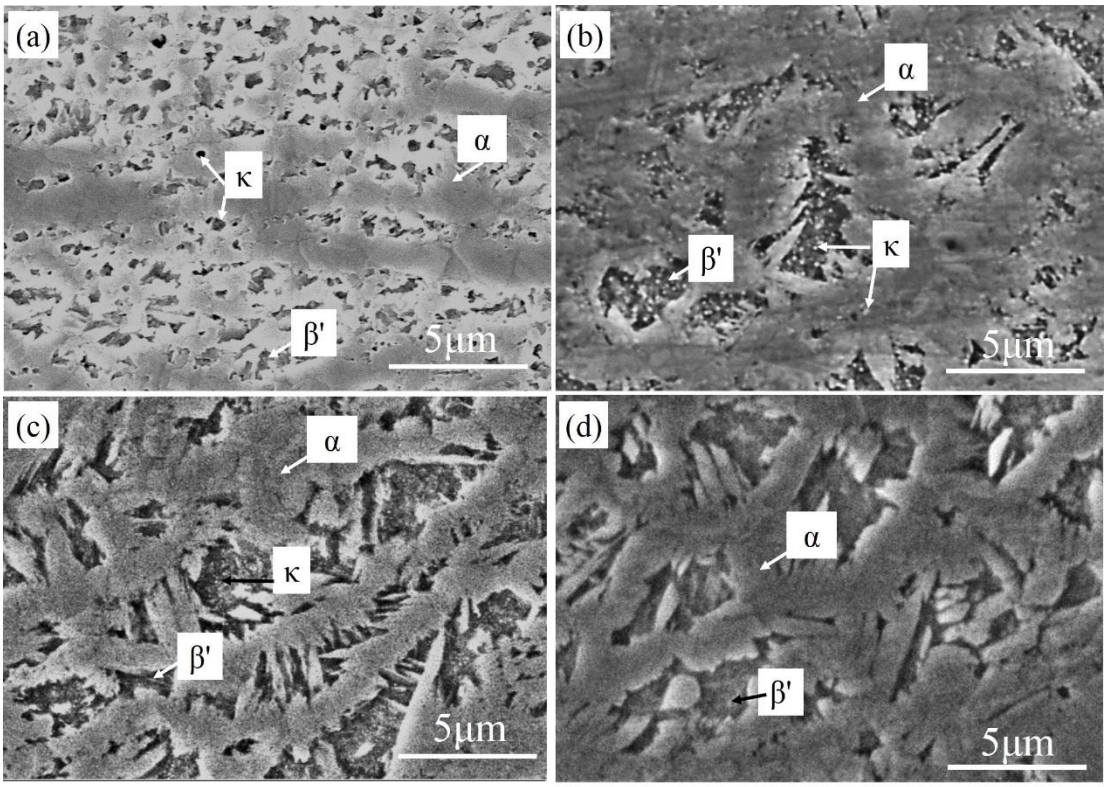

Fig. 2 SEM images of friction stir processed NAB alloy samples. (a) FSP600, (b) FSP800, (c) FSP1000, (d) FSP1200.

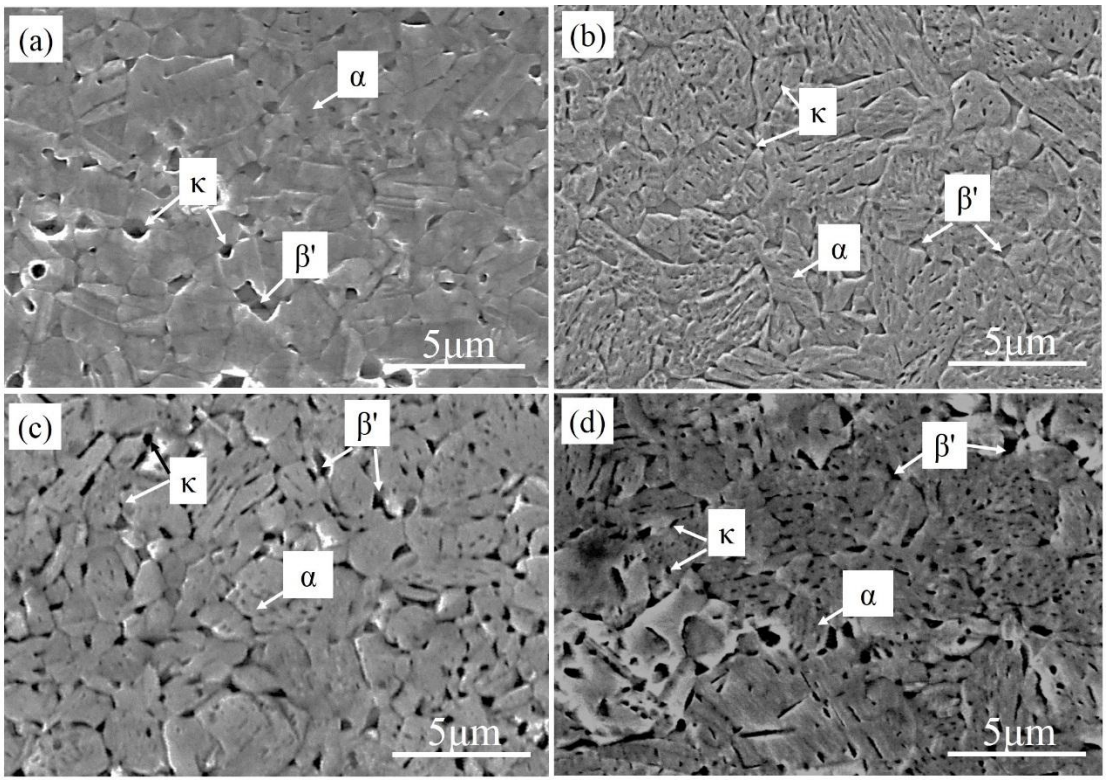

Fig. 3 SEM images of post heat treated NAB alloy samples. (a) PHT600, (b) PHT800, (c) PHT1000 and (d) PHT1200.

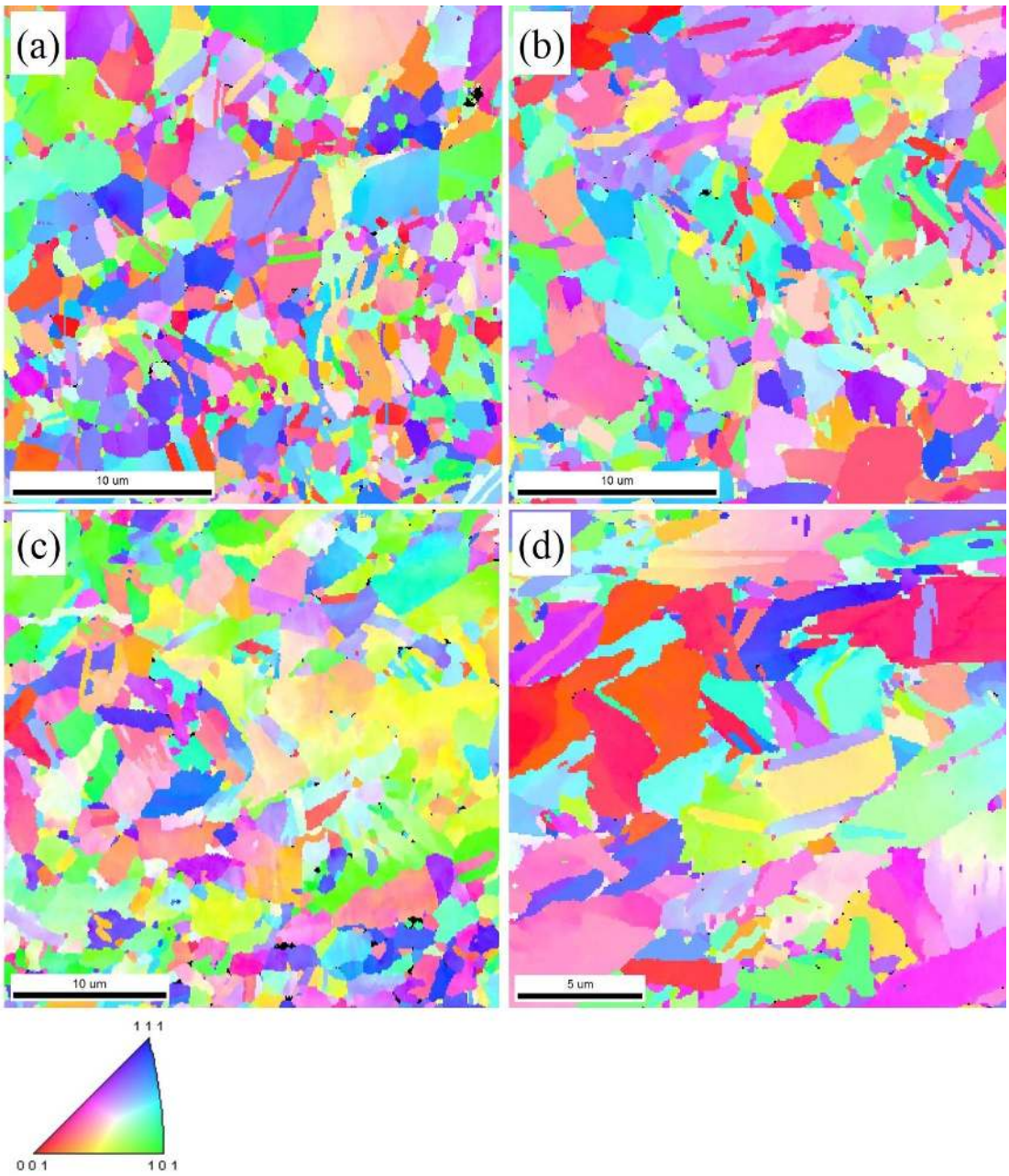

Fig. 4. EBSD-IPF maps of post heat treated NAB alloy at different rotation rates. (a) PHT600, (b) PHT800, (c) PHT1000 and (d) PHT1200.

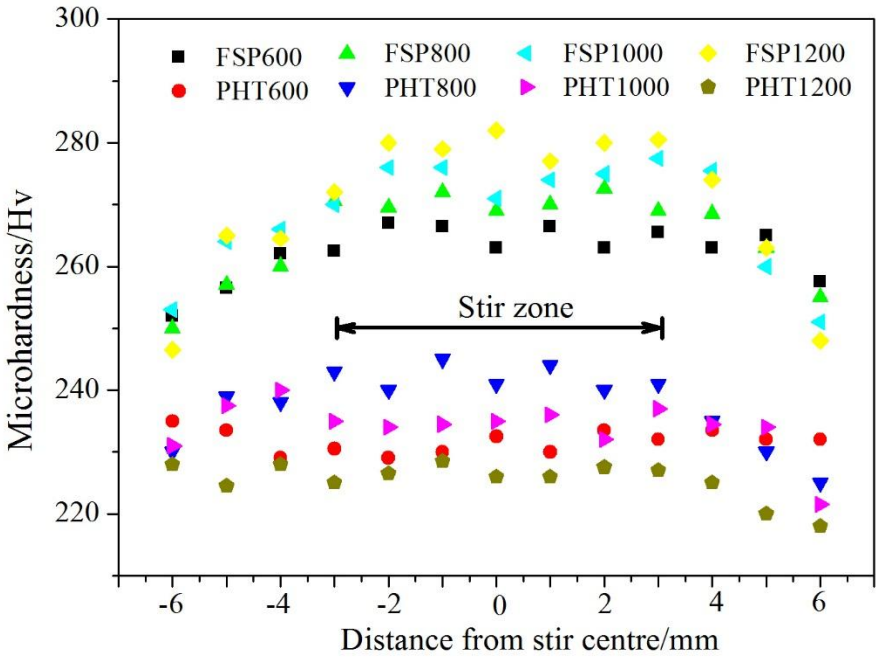

Fig. 5 Microhardness distribution map of stir zone in friction stir processed and post heat treated NAB alloy with various rotation rates.

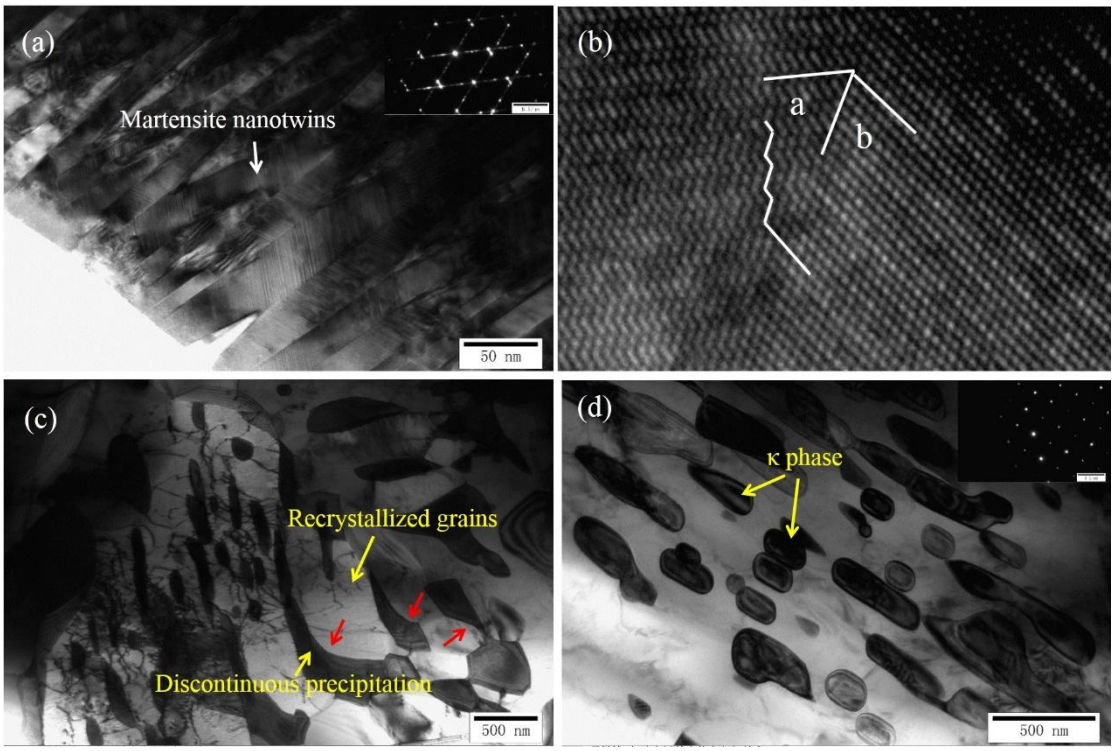

Fig. 6 TEM images of FSP1000 and PHT1000 samples. (a) Nano-twins, (b) HRTEM image of a typical type of twinning morphology in Fig. 6(a). (c) and (d) The transformation of β' phase during post heat treatment. Inset in Fig. 6(a) is electron diffraction pattern of nanatwins. Inset in Fig. 6(d) is electron diffraction pattern of black precipitations.

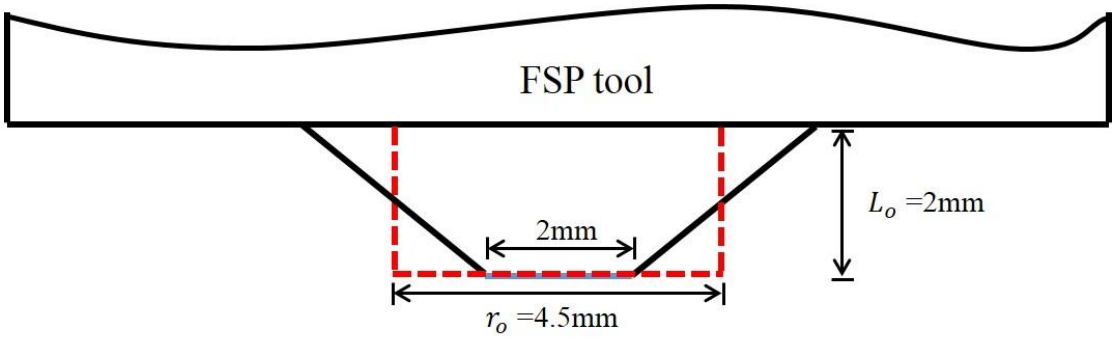

Fig. 7 Schematic drawing showing the dimension of FSP tool.

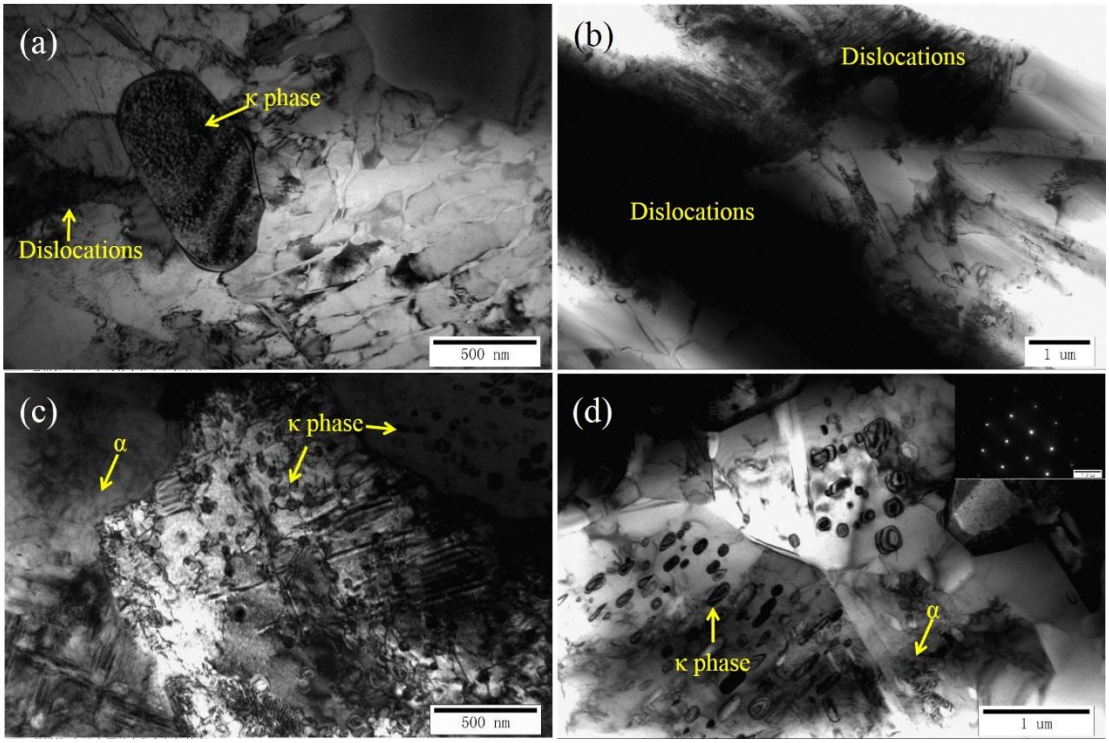

Fig. 8 TEM images of the friction stir processed and post heat treated NAB alloy: (a) FSP600, (b) FSP1000, (c) FSP800, (d) PHT800. Inset in Fig. 8(d) is electron diffraction pattern of black precipitations.

Table 1. Relative volume fraction (V_f) of α and κ phases in post heat treated NAB alloys

Sample	α phase V_f (%)	κ phase V_f (%)
PHT600	93.8	6.2
PHT800	94.9	5.1
PHT1000	93.3	6.7
PHT1200	93.9	6.1